AIAA 97-0098
An MDO Investigation of the Impact of Practical Constraints on an HSCT Configuration

P.E. MacMillin, O. Golovidov,
W.H. Mason and B. Grossman
Virginia Polytechnic Institute and
State University, Blacksburg, VA

and

R.T. Haftka
University of Florida
Gainesville, FL

35th Aerospace Sciences Meeting & Exhibit
January 6-9, 1997 / Reno, NV

An MDO Investigation of the Impact of Practical Constraints on an HSCT Configuration

Peter E. MacMillin*, Oleg B. Golovidov†, William H. Mason‡,
Bernard Grossman§, and Raphael T. Haftka¶

Multidisciplinary Analysis and Design (MAD) Center for Advanced Vehicles
Virginia Polytechnic Institute and State University
Blacksburg, Virginia 24061

This paper presents results from an MDO design procedure illustrating the effects of numerous trim, control, and performance requirements for a high speed civil transport. We optimize the design for minimum take off gross weight, including both aerodynamics and structures to find the wing planform and thickness distribution, fuselage shape, engine placement and thrust, using 29 design variables and 70 constraints to insure realistic results. The constraints include the engine-out and crosswind landing requirements, as well as engine nacelle ground strike, rotation to lift-off attitude, balanced field length and approach trim constraints. We found that the engine-out condition and the engine nacelle ground strike avoidance were critical conditions. The addition of a horizontal tail to allow take-off rotation resulted in a significant weight penalty. We also examined the effect of engine technology and sizing based on cruise and balanced field length constraints. The field length has a large influence on weight. We included a subsonic leg in our mission analysis, which also resulted in a large weight penalty. The cumulative effect of these considerations leads to very large increases in vehicle weight. We conclude with sensitivity studies performed to understand the effect of some of the constraints and the accuracy of the drag prediction on the optimized results.

1. Introduction

Supersonic transport design is extremely demanding. Many of the mission requirements conflict with one another. To satisfy all of the requirements, the designer must completely integrate the various requirements and technologies in the design, such as trading supersonic cruise efficiency for takeoff and landing performance. The efficiency and economic feasibility of the final design is determined by the quality of the technology integration.

Multidisciplinary design optimization (MDO) is a means of achieving the required system integration. For vehicles designed for extremely demanding missions, MDO is an enabling technology, without which the design goals will not be achieved. Sobieski has provided much of the impetus for this approach and has written the key reviews describing MDO[1-3].

The key challenges in achieving a viable MDO procedure for a complete vehicle are due to the increase in the number of design variables and the associated computational cost compared to single discipline optimization, and the increased complexity of the software engineering problem. An overview of our group's understanding of MDO for advanced vehicle design and a description of our research effort has been presented in a survey paper by Giunta *et al.*[4] That paper reflects the experience gained over a number of years, most recently using the HSCT as the focus of the work, *e.g.* Refs. 5 - 9. The key consideration has been the balance between the fidelity of the methodology used to represent the various single disciplines and the reality of using the single discipline results in a practical MDO procedure. At Virginia Tech, variable-complexity modeling has been used to develop a practical procedure. The exact nature of this modeling has evolved as we have gained experience.

Other approaches to the MDO problem are also being developed. These include the work by the groups at Stanford,[10-12] Georgia Tech,[13, 14] and Notre Dame.[15] In industry and government the em-

*Graduate Research Assistant, Dept. of Aerospace and Ocean Engineering, Student Member AIAA, now at Lockheed Martin, Palmdale, CA

†Graduate Research Assistant, Dept. of Aerospace and Ocean Engineering, Student Member AIAA

‡Professor of Aerospace and Ocean Engineering, Associate Fellow AIAA, mason@aoe.vt.edu

§Professor and Head, Dept. of Aerospace and Ocean Engineering, Associate Fellow AIAA

¶Professor of Aerospace Engineering, Mechanics and Engineering Science, University of Florida, Gainesville, FL, Associate Fellow AIAA

phasis has mainly been on increased fidelity of the disciplinary models.[16, 17]

In this paper we focus on one area where the computational problem is acute: combined aerodynamic-structural-controls-propulsion design of the high speed civil transport (HSCT). Here we apply the methodology of Hutchison *et al.*[5–7] and its extension to include control considerations by MacMillin *et al.*[9] to study the effect of the mission requirements and trim, control and propulsion constraints. The ability to address realistic constraints is critical in developing a practical MDO procedure. Note that we are illustrating the effects of constraints on an HSCT using the MDO methodology we propose for use in actual design. However we do not suggest that our results should replace those of the large design teams working in industry and government.

Constraints to be considered in this paper are: engine out and cross-wind landing, engine thrust, approach trim, nacelle/wingtip scrape, and aircraft rotation and balanced field length takeoff distance (BFL). We will present results showing sensitivity to engine technology, subsonic mission distance, BFL, and the drag predictions. The sensitivity to drag prediction is important because of the need to understand the role of linear theory, Euler and Navier-Stokes prediction methods in MDO design procedures.[18]

The results were obtained using the final code from our original variable-complexity modeling approach.[19] The weights are found using the FLOPS weight equations,[20] and the aerodynamic performance is computed directly using both simple and detailed analysis methods. The detailed analyses for this work consist of various panel-level approximations and boundary layer estimates. The stability and control derivatives are computed using algebraic formulas that are updated every five iteration cycles with a more detailed analysis[21, 22] using the so-called interlacing concept, which has also been applied to the wing weight equations by Dudley *et al.*[8]

This approach has been found to work reasonably well. However, numerical noise generated by analysis codes degrades convergence and results in some uncertainty in the results due to the possibility of becoming trapped in artificial local minima.[23] As a result, new approaches which reduce the numerical noise problem and exploit the use of parallel computing are emerging.[4]

The results presented here illustrate the importance of including realistic constraints in MDO procedures and serve as a benchmark for the new methods currently under development, including the use of response surface methods for the aerodynamics,[23] the structural weight,[24] and the nonlinear pitching moments.[25] The new method has the goal of improving convergence, avoiding local minima, reducing computational cost, and allowing the use of improved disciplinary models without having to couple large codes directly.

In the next section we discuss the design issues addressed in this work. Section 3 describes how we formulate our design problem. Variable-complexity modeling is explained in detail in section 4. Our analysis methods are described in section 5. In section 6 we present our results by showing a succession of optimizations. Each optimization incorporates new requirements and shows the effect of the new requirements on the design. Sensitivity study results are also presented in this section. Finally, we discuss our conclusions in section 7.

2. Design Issues

2.1. Control and Stability

Although the MDO problem focuses on vehicle performance, almost every component's size and location is dictated by a critical constraint, many of which are associated with control requirements. Explicit consideration of trim and control in conceptual aircraft sizing methodology is unusual. For subsonic configuration optimizations there have been related studies by Sliwa[26, 27] and by Gallman *et al.*[11] Both considered longitudinal trim and control, and both found that including trim and control considerations affected the design. Control requirements specific to HSCT configurations have recently been examined by McCarty *et al.*[28] Based on that work, together with our own, we use the subsonic (low dynamic pressure) field performance requirements as the critical control requirements condition.

In addition to static requirements, flight control system design is also an important consideration for modern vehicles. Flying qualities considerations in MDO design have been introduced by Anderson and co-workers.[29, 30] Although not implemented here, it produces a direct means of incorporating control system design in an MDO procedure.

2.2. Vertical Tail Sizing

For civilian aircraft with four engines, where maneuverability is not a primary consideration, the vertical tail size is based either on the requirement that the aircraft be capable of trimmed flight with two

engines inoperative as specified in FAR 25.147, or to handle the crosswind landing requirement. Therefore, we require the aircraft be trimmed directionally using no more than 75% of the maximum available control authority.

The magnitude of the yawing moment required to trim the engine out condition depends on the thrust of the engines, and their spanwise positions. The crosswind landing condition requires the aircraft balance the yawing moment caused by a 20 *knot* crosswind, as specified in FAR 25.237. Deflecting the rudder creates the balancing yawing moment, but also causes a sideforce which must be counteracted. This is done with a combination of sideslip and bank. Both sideslip and bank can make landing difficult if the angle is too great. Excessive bank introduces the possibility of the wing tip scraping the ground before the landing gear touches down. Thus, the allowable amount of sideslip and bank are limited to 10° and 5°, respectively.

2.3. Engine Location Limits

Moving the engine outboard provides wing bending moment relief, thereby reducing the wing weight. As the engine moves outboard, the vertical tail must increase in size to satisfy the engine out condition. But, the increase in vertical tail weight is small compared to the reduction in wing weight, as shown in Fig. 1. There is a practical limit to the amount of wing bending moment relief moving the engine outboard can produce. After this limit is reached, moving the engine further outboard does not result in any further reduction in wing weight. But vertical tail size and weight continue to increase. This produces a minimum in the sum of the wing and vertical tail weights at the point where the limit is reached.

The increase in drag due to increasing the vertical tail size and including the associated movement of the nacelle is small, as shown in Fig. 2. The increase in volumetric wave drag is less than two counts, and the increase in friction drag is about three counts. Thus the minimum takeoff gross weight (TOGW) is achieved with a very large vertical tail and with engine placement at the point where the limit in wing bending moment relief is achieved. Placing the engine extremely far outboard could cause problems with flutter, engine-out trim, nacelle strike during landing, and airframe stresses during ground operations, such as full fuel taxi. A constraint is needed to prevent the optimizer from placing the engines too far outboard on the wing.

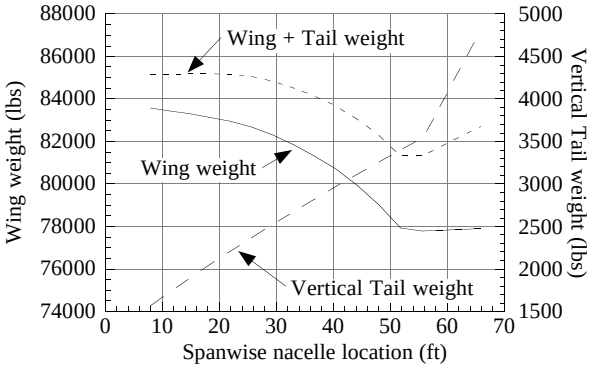

Figure 1: The sum of the wing and vertical tail weights decreases as the engine is moved outboard. (Note different scales for wing weight and vertical tail weight)

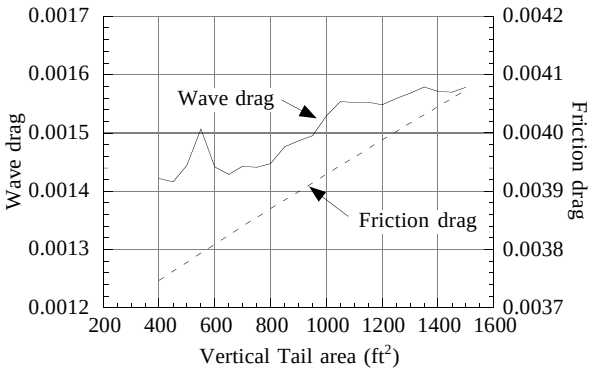

Figure 2: The wave drag increases very little with nacelles moving outboard and increasing vertical tail area.

2.4. Nacelle and Wing Tip Strike

Due to the low lift curve slope of HSCT configurations, which results in high landing angles of attack, approximately 12°, it is possible for the engine nacelles to strike the runway. This is dependent on the positioning of the nacelles and the sweep of the wing trailing edge, as well as the length and position of the landing gear. An allowance must also be made for up to 5° of bank.

A similar problem exists with the wing tips. A large amount of trailing edge sweep can place the trailing edge of the wing tip well behind the main gear. When this is coupled with the relatively high landing angle of attack and even a small amount of bank, it can cause the wing tips to strike the runway.

2.5. Landing Gear Location

Landing gear integration is also an important consideration.[31] Its position relative to the center

of gravity is important for take-off rotation, as well as the effect on the engine nacelle strike constraint. Both the nose and main gear positions must be known to compute the center of gravity location. On landing, the main gear touches down first, so the position and length of the main gear is critical to the nacelle and wing tip strike constraints.

The weight distribution on the landing gear is important during take-off rotation. If the nose gear is too heavily loaded, it will be difficult to rotate to the take-off attitude. If the nose gear is too lightly loaded, the aircraft will be hard to steer and could rotate before there is enough control authority to control the aircraft's attitude. Torenbeek[32] recommends the nose gear support between 8% and 15% of the total weight. We elected to place the nose gear so that it would be supporting 11.5% of the total weight.

Other important considerations include the tipback and overturn angles. Both angles relate the main gear's position to the location of the center of gravity. The tipback angle is the angle between the main gear and the *cg* as seen in the side view, and it should be 15° or less. If the main gear is not far enough behind the center of gravity, the aircraft could tip back on its tail. As the tipback angle is increased, the pitching moment required to rotate the aircraft for takeoff also increases. The horizontal tail size is very sensitive to this parameter. The overturn angle is a measure of the likelihood of the aircraft tipping over sideways while taxiing in a turn. It should be less than 63°. A complete discussion can be found in Ref. 19.

2.6. Horizontal Tail Sizing

Several longitudinal control and trim issues are important. The field performance requirements are among the most critical. For most airplanes, take-off involves rotating on the main landing gear to a pitch attitude at which the wings can generate enough lift to become airborne. The civilian FAR[33] regulations require the aircraft be able to take off safely. If the takeoff rotation requires too much time, it will greatly increase the takeoff distance. This limits the number of airports that the aircraft can use. We require the aircraft be able to rotate to lift-off in under 5 *sec**.

*This requirement was determined by investigating typical rotation times for large aircraft. Since there are very few aircraft of this type there is not a large body of data to base our requirement on. Requiring the aircraft to rotate in under 5 *sec* is a somewhat arbitrary but reasonable assumption. This constraint was incorporated into the code before take-off distance calculation was developed and included. The effect of this assumption is described below.

Approach trim is also important. The aircraft must be able to be trimmed at an angle of attack well above normal operating conditions. There should also be enough additional control power beyond trim to maneuver. This allows the pilot to deal with gusts and emergencies. For unstable aircraft, the amount of nose down pitching moment available at high angle of attack required for safe flight is a current research topic.[34]

2.7. High Lift Systems

Consideration of takeoff and landing constraints requires consideration of high lift system effects. In this study we use "typical" increments for lift and pitching moment due to the use of a high lift system, as collected in a survey of wind tunnel test results by Benoliel and Mason.[35, 36] This is an approximate model, in that the effects are assumed to be independent of the planform shape. In this work we use a constant 30° trailing edge flap deflection. Subsequent work by Crisafulli *et al.*[25] used an improved model for the high lift system, wherein response surface models were constructed that do take into account effects of planform shape changes.

2.8. Engine Sizing

Engine size is determined primarily by bypass ratio and the maximum massflow the engine is required to handle. The maximum massflow is proportional to the maximum thrust the engine can produce. So, for a given bypass ratio, the size of the engine is based on the maximum thrust required.

One of the determining factors for engine thrust is the takeoff distance requirement. The second segment climb requirements are sometimes the critical conditions for sizing the engine. Also, the thrust available during flight must be sufficient to overcome drag. It is desirable to use the smallest engine possible, while satisfying all of the mission requirements.

3. Design Formulation

Our design problem is to optimize an HSCT configuration to minimize TOGW for a range of 5500 n.mi., and 251 passengers. Our main mission is a supersonic cruise-climb at Mach 2.4 with a maximum altitude of 70,000 *ft*. In this work, we expand our mission to include take off, and a subsonic cruise at Mach 0.9.

The choice of gross weight as the figure of merit (objective function) directly incorporates aerodynamic, structural and propulsion considerations, in that

the structural design directly affects aircraft empty weight and drag, while aerodynamic performance dictates the required fuel weight. Both affect the size of the engine required. Trim and control requirements are explicitly treated also. The current work incorporates the influence of structural considerations in the aerodynamic design by a variable-complexity modeling approach. We employ the weight equations of McCullers.[20] A procedure called *interlacing* is used to estimate stability and control derivatives. Variable-complexity modeling and interlacing will be described in Section 4.

3.1. Design Variables

A key problem in MDO is to characterize the complete configuration with relatively small number of design variables. For the level of analysis considered here, costs limit this number to be small, typically below 100. We have achieved this goal for a complex wing-body configuration by selecting a few parameters which contain the primary effects required to provide flexible, realistic parametric geometry. The model we have developed completely defines the configuration using 29 design variables. While the configuration is defined using this set of parameters, the aircraft geometry is actually stored as a discrete numerical description in the Craidon format.[37]

The variables fall into seven categories: wing planform, airfoil, nacelle placement, engine thrust, fuselage shape, mission variables, and tail areas. Table 1 presents the set of design variables.

The eight design parameters used to define the planform are shown in Fig. 3. The leading and trailing edges of the wing are defined using a blending of linear segments, as described in Ref. 38. The airfoil sections have round leading edges. We define the thickness distribution using an analytic description.[39] It is defined by four parameters: the thickness-to-chord ratio, t/c, the leading-edge radius parameter, I, the chordwise location of maximum thickness, m, and the trailing-edge half angle, τ_{TE}; see Fig. 4. The thickness distribution at any spanwise station is then defined using the following rules:

1. The wing thickness-to-chord ratio is specified at the wing root, the leading-edge break and the wing tip. The wing thickness varies linearly between these control points.

2. The chordwise location of the maximum airfoil thickness is constant across the span.

Table 1: Design Variables

Number	Baseline Value	Description
1	142.01	Wing root chord *(ft.)*
2	99.65	L.E. break, x *(ft.)*
3	28.57	L.E. break, y *(ft.)*
4	142.01	T.E. break, x *(ft.)*
5	28.57	T.E. break, y *(ft.)*
6	138.40	L.E. wing tip, x*(ft.)*
7	9.30	Wing tip chord, *(ft.)*
8	67.32	Wing semi-span, *(ft.)*
9	0.50	Chordwise max t/c location
10	4.00	L.E. radius parameter
11	2.96	Airfoil t/c at root, %
12	2.36	Airfoil t/c at L.E. break, %
13	2.15	Airfoil t/c at tip, %
14	70.00	Fuselage restraint 1, x *(ft.)*
15	6.00	Fuselage restraint 1, r *(ft.)*
16	135.00	Fuselage restraint 2, x*(ft.)*
17	5.80	Fuselage restraint 2, r*(ft.)*
18	170.00	Fuselage restraint 3, x*(ft.)*
19	5.80	Fuselage restraint 3, r*(ft.)*
20	215.00	Fuselage restraint 4, x*(ft.)*
21	6.00	Fuselage restraint 4, r*(ft.)*
22	17.79	Nacelle 1, y *(ft.)*
23	32.07	Nacelle 2, y *(ft.)*
24	290,905	Mission fuel, *(lbs.)*
25	50,000	Starting cruise altitude, *(ft.)*
26	100.00	Cruise climb rate, *(ft/min)*
27	450.02	Vertical tail area, (ft^2)
28	750.00	Horizontal tail area, (ft^2)
29	46,000	Maximum sea level thrust per engine, *(lbs)*

3. The airfoil leading-edge radius parameter is constant across the wing span. The leading edge radius-to-chord ratio, r_t, is defined by $r_t = 1.1019\left[(t/c)\,(I/6)\right]^2$.

4. The trailing-edge half-angle of the airfoil section varies with the thickness-to-chord ratio according to $\tau_{TE} = 3.03125(t/c) - 0.044188$. This relationship is fixed throughout the design.

The spanwise nacelle locations vary during the optimization process. However, we fix the axial location of the nacelles in relation to the wing's trailing edge, using a value of 25% overhang. Another design variable specifies the maximum engine thrust. The nacelle diameter and length are scaled by the square

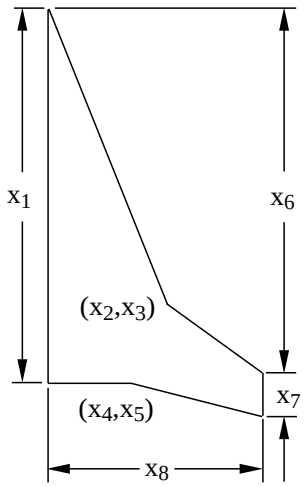

Figure 3: Planform Definition Parameters

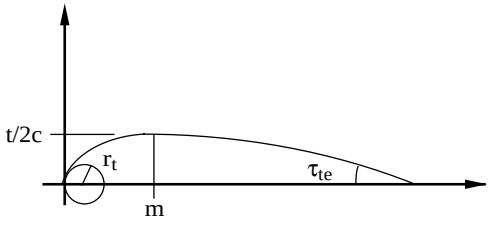

Figure 4: Airfoil Thickness Parameters

root of the ratio of current thrust to baseline thrust. The weight of the engine is also a function of this ratio.

The fuselage is assumed to be axisymmetric, but area ruled. The axial location and radius of each of four *restraint* locations are the design variables.[7] We define the shape of the fuselage between these restraints by requiring that it be a minimum wave-drag body for the specified length and volume.[40] The vertical tail and horizontal tail are trapezoidal planforms. For each of these control surfaces, the aspect ratio, taper ratio, and quarter-chord sweep are specified, and the area varies.[9]

Three variables define the idealized cruise mission. One variable is the mission fuel and the other two specify the Mach 2.4 cruise in terms of the initial supersonic cruise altitude and the constant climb rate used in the range calculation. The resulting aircraft range is calculated using the fuel weight design variable, assuming that 85% of the mission fuel is used in cruise and the remaining 15% is the reserve fuel.

3.2. Constraints

The constraints used in the problem fall into three categories: constraints implicit in the analysis, performance/aerodynamic constraints, and geometric constraints. The implicit constraints are not handled by the optimization program, but rather are part of the analysis or geometry:

1. The maximum altitude, 70,000 *ft*, is enforced in the range calculation.
2. The fuselage volume is fixed at 23,270 ft^3 and the fuselage length is fixed at 300 *ft*.
3. The axial location of the wing's MAC quarter chord is adjusted to match the value found on the baseline configuration (147.3 *ft* aft of the aircraft nose).
4. The nacelles are fixed axially as noted in Section 3.1 above. In the studies done with engine thrust fixed at 39,000 *lbs*, the nacelles are approximately 27 *ft* long and 5 *ft* in diameter. When the thrust is allowed to vary, the baseline thrust is 46,000 *lbs*, the baseline length and diameter are 35 *ft* and 6.5 *ft*, respectively.

Aside from these implicit constraints we also use up to 70 explicit constraints, summarized in Table 2. The range is constrained to be 5500 *n.mi.* or more. The C_L at landing speed must be less than 1, the C_ℓ for each of the 18 wing sections must be less than 2 (an elliptic load distribution is used), and the landing angle of attack is constrained to be less than or equal to 12°. The mission fuel must not require more space than the available fuel volume, which we assume to be 50% of the total wing volume.

Another group of constraints is designed to keep the optimizer from developing geometrically impossible or implausible designs. For example, a constraint is used to prevent the design of a wing which is highly swept back into a spiked shape. In this category are the thickness-to-chord constraints, without which the optimizer could attempt to create a wing with negative thickness. The constraint numbered 51 forces the wing's trailing edge to end before the horizontal tail's leading edge begins. Constraints 64 and 65 require nacelle 1 to be outboard of the fuselage and inboard of nacelle 2. Constraint 66 requires the aircraft trim with two engines out if the vertical tail is included in the optimization; otherwise the outer nacelle limit is fixed at 50% semi-span.

Trim and control considerations require 11 constraints: numbers 42–50, 53 and 66 in Table 2, most of which are related to landing. The landing constraints are enforced for assumed emergency conditions, i.e. a landing altitude of 5,000 *ft* with an out-

Table 2: Optimization Constraints

Number	Description
1	Range $\geq$ 5,500 *n.mi.*
2	Required C_L at landing speed ≤ 1
3-20	Section $C_\ell \leq 2$
21	Landing angle of attack $\leq 12°$
22	Fuel volume $\leq$ half of wing volume
23	Spike prevention
24-41	Wing chord $\geq$ 7.0 *ft.*
42-45	Engine scrape at landing
46	Wing tip scrape at landing
47	Rudder deflection for crosswind landing $\leq 22.5°$
48	Bank angle for crosswind landing $\leq 5°$
49	Takeoff rotation to occur ≤ 5 *sec* [a]
50	Tail deflection for approach trim $\leq 22.5°$
51	Wing root T.E. $\leq$ horiz. tail L.E.
52	Balanced field length $\leq 10,000$ *ft* [a]
53	T.E. break scrape at landing with 5° roll
54	L.E. break $\leq$ semispan
55	T.E. break $\leq$ semispan
56-58	Root, break, tip $t/c \geq 1.5\%$
59-63	Fuselage restraints in order
64-65	Nacelles in order
66	Engine-out limit with vertical tail design; otherwise 50%
67-70	Maximum thrust required $\leq$ available thrust

[a] Sensitivity to these constraints is examined in Section 6.6

side temperature of 90° F, and with the aircraft carrying 50% fuel. The vertical tail is sized based on either the requirement that the aircraft be capable of trimmed flight with two engines on the same side inoperative or to meet the 20 *kt* crosswind landing requirement. The pilot must have sufficient control authority to trim the aircraft in these situations, as well as to be able to perform necessary maneuvers safely. Therefore, we require the aircraft be trimmed directionally using no more than 75% of the available control authority and limit bank to 5°. For the engine-out condition these constraints are implicit in the analysis. For the crosswind landing requirements these are explicit in constraints 47 and 48.

The engine nacelle strike constraint requires that the nacelles not strike the runway during landing, which limits the allowable spanwise engine location. This is checked at main gear touch down, with the aircraft at the landing angle of attack and 5° bank, the typical certification requirement. This constraint not only limits the spanwise engine location, but effectively limits the allowable trailing edge sweep, because the nacelles are mounted at the trailing edge, with 25% overhang. Another constraint checks wing tip strike under the same conditions. During the crosswind landing, the aileron and rudder deflections are limited to 75% of maximum, or 22.5°, and the bank must be less than 5°.

Constraints on take-off rotation time (no. 49), balanced field length (no. 52) and approach trim (no. 50) determine the size of the horizontal tail. We require the aircraft rotate to lift-off attitude in less than 5 *seconds*. For the approach trim, the aircraft must trim at the approach attitude with a horizontal tail deflection of less than 22.5°.

The constraint on the balanced field length insures the aircraft can operate from existing airports. Requiring the BFL be less than 10,000 *ft* allows the aircraft to use most major airports in the world. This constraint limits the maximum wing loading and the minimum thrust to weight ratio. HSCT TOGW sensitivity to this constraint is examined below. The final four constraints require the maximum thrust required in each segment of the mission be less than the thrust that is actually available at the given flight condition.

4. Variable Complexity Modeling and Optimization

A growing practice in MDO is the use of approximation associated with what we term variable-complexity modeling (VCM). For example, the structural design of an aircraft is often performed with a complex structural model, but with loads obtained from simple aerodynamic models. Similarly, the aerodynamic designer may use advanced aerodynamic models with a simple structural model to account for wing flexibility effects.

We employ a VCM approach using both the simple and complex models during the optimization procedure. Our aim is to take advantage of the low computational cost of the simpler models while improving their accuracy with periodic use of the more sophisticated models. The sophisticated models provide scale factors for correcting the simpler models. These scale factors are updated periodically during the design process. For example, in Ref. 5 we combined the use of simple and complex aerodynamic models to predict the drag of an HSCT during the optimization process. Similarly, in Ref. 8 we employed structural optimization together with

a simple weight equation to predict wing structural weight in combined aerodynamic and structural optimization of the HSCT. We have also used this approach to handle the estimation of stability and control derivatives.[9]

The variable-complexity modeling approach is used within a sequential approximate optimization technique whereby the overall design process is composed of a series of optimization cycles. We use NEWSUMT[41] in this work. Each optimization cycle is performed using approximate analysis. At the beginning of each cycle, approximations are constructed using either scaled, global-local or interlacing approximations. The optimization converges using only the approximate analysis, but move limits are imposed on the design variables to limit the discrepancies between the approximate and the complex analysis. These discrepancies result in constraint violations. The approximations must be updated and the design must be refined by continuing the optimization. This process continues until the design converges and the constraints are satisfied.

The scaled approximation employs a constant scaling function $\sigma(\mathbf{x})$, where $\mathbf{x}$ represents a vector of design variables, given as

$$\sigma(\mathbf{x_0}) = \frac{f_d(\mathbf{x_0})}{f_s(\mathbf{x_0})}. \tag{1}$$

In this expression f_d represents a detailed model analysis result, and f_s represents a simple model analysis result, both evaluated at a specified design point, $\mathbf{x_0}$, at the beginning of an optimization cycle. During an optimization cycle the scaled approximate analysis results, $f(\mathbf{x})$, are calculated as

$$f(\mathbf{x}) \approx \sigma(\mathbf{x_0}) f_s(\mathbf{x}). \tag{2}$$

Thus, the scaled simple analysis is used throughout the cycle until convergence. Then a new value of the scale factor is computed and the optimization is repeated. Move limits are imposed during the optimization cycles.

A procedure which varies the scale factor during the optimization cycles is called the global-local approximation technique. The approximation is again constructed from the simple model

$$f(\mathbf{x}) \approx \sigma(\mathbf{x}) f_s(\mathbf{x}) \tag{3}$$

with the scaling parameter approximated using

$$\sigma(\mathbf{x}) \approx \sigma(\mathbf{x_0}) + \nabla\sigma \cdot (\mathbf{x} - \mathbf{x_0}) \tag{4}$$

The gradient of σ at $\mathbf{x_0}$ is performed by forward finite differences involving both f_d and f_s. In our aerodynamic analysis we have used the scaled approximation for the drag due to lift and the global-local for the wave drag.[5, 7]

For more expensive analyses the scaled approximation is used, but with the scale factor updated only every fifth cycle. This procedure, called interlacing, is used for estimating the stability and control derivatives. The complex model is used after every five optimization cycles. (The choice of five is somewhat arbitrary). The stability derivatives calculated by the complex model are used to provide scale factors for the next five optimization cycles. Interlacing has also been used by Dudley *et al.*[8] for estimating wing weight.

5. Analysis Methods

We continue to use the aerodynamic drag analysis and representation of the wing structure using weight equations used previously. Detailed descriptions of these can be found in Refs. 5 - 7. The so-called detailed aerodynamics calculations are based on the vortex lattice method,[42] the Mach box method,[43, 44] and the Harris wave drag code.[45] A simple strip boundary layer correction is implemented as in Ref. 5.

To analyze trim and control conditions it is necessary to obtain information not normally used in initial sizing programs. This includes the location of the center of gravity (cg), the inertias, and the stability and control derivatives. These are found for a given geometry and flight condition.

We use two techniques to estimate the stability and control derivatives; empirical algebraic relations from the U.S.A.F. Stability and Control DATCOM[46], as interpreted by J. Roskam[47], and a VLM code developed by Kay.[22] The DATCOM methods rely on simple theories and some experimental data, and do not handle unusual configurations well. The VLM code is better able to handle different configurations, but is more expensive computationally. A detailed description of these techniques is given in Ref. 19.

6. Results

In this section, we describe the results of a number of MDO design studies. First, we discuss the baseline case with no vertical or horizontal tail sizing. Then, two studies with vertical tail sizing using slightly different starting conditions are presented as Case 27a and Case 27b, followed by two studies with vertical and horizontal tail sizing as Case 28a and

Table 3: Cases with Various Constraints

Case	Constraint
26a	Baseline
27a	Same as 26a, but add vertical tail sizing
27b	Same as 27a, but change initial starting conditions
28a	Add horizontal tail sizing
28b	Same as 28a, but degrade engine performance
29a	Same as 28b, but add engine sizing
29b	Same as 29a, but add subsonic leg

Table 4: Cases Studying Sensitivities

Case	Sensitivity
29c	Effect of BFL constraint
29x	Effect of drag prediction (+/- 1, 2 counts)
29d	Effect of rotation time constraint

Case 28b. Case 28b shows the effect of engine technology. Then we discuss Case 29a with engine sizing and Case 29b with all of the above and a subsonic leg added to our mission. Table 3 lists the cases and charts the progression of the studies. The case number corresponds to the number of design variables used.

Several sensitivity studies follow the main results in Section 6.6. Table 4 shows the cases that were investigated during the sensitivity studies. First we describe the effects of relaxing the BFL on the HSCT (Case 29a is taken as the basis for this case with changed BFL limit), then the sensitivity of TOGW to the drag coefficient value and finally, the role of the rotation time constraint on the HSCT configuration and weight.

6.1. Baseline Optimization (Case 26a)

Case 26a is used as the baseline case. It has 26 design variables, and 62 constraints. Constraints numbered 47-52, 69 and 70 in Table 2 were not used in this case. The mission is entirely supersonic, the vertical tail is fixed in both size and shape, and there is no horizontal tail.

The initial design violated three constraints, the range constraint and the two thrust constraints. After 30 optimization cycles, the TOGW has been reduced by 34,200 *lbs* and all of the constraints are now satisfied. The convergence history of the TOGW is shown in Fig. 5. The initial and final planforms are shown in Fig. 6 and Table 5 compares the two designs.

The final design has an unusual planform, with the inboard trailing edge swept forward. The optimizer moved immediately to this design, and this change reduced the wing weight by about 14,000 *lbs*. Due to the lower aspect ratio, the drag due to lift does increase, but this is offset by a reduction in volumetric wave drag. Overall, the total drag decreases slightly by the end of the optimization.

The initial design has a wing loading of 63.68 *psf*. In the final design the wing loading has been reduced to 56.30 *psf*. Lowering the aspect ratio improves the supersonic efficiency, but it also lowers the lift curve slope. This means that for a given wing area, the aircraft would have to fly at a higher angle of attack to generate the same lift. To keep from violating the 12° angle of attack constraint the optimizer increased the wing area, which decreased the wing loading.

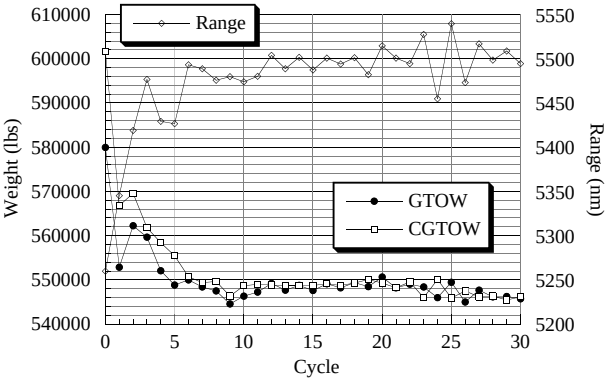

Figure 5: Convergence of Case 26a

6.2. Vertical Tail Considerations

These optimizations include the vertical tail sizing, and require 27 design variables with 64 constraints. Constraint number 66 is changed to the engine out limit from the arbitrary limit of 50% of the semispan, and constraints 47 and 48 are added for the crosswind landing. Again, the mission is entirely supersonic, and there is no horizontal tail, but the vertical tail is allowed to vary in size.

6.2.1. Case 27a

The same initial design is used as in Case 26a, with the exception that the initial value of the starting altitude was changed from 50,000 *ft* to 60,000 *ft*, and the climb rate was changed from 100 *ft/sec* to

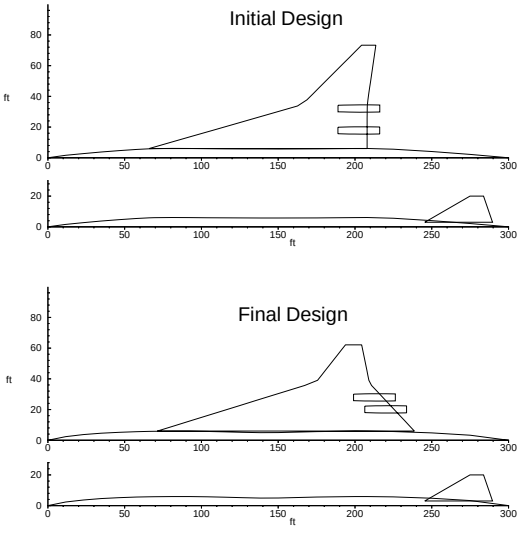

Figure 6: Initial and final planforms, Case 26a

Table 5: Comparison of Initial and Final Designs, Case 26a

	Initial	Final
Gross Weight (*lbs*)	580,000	545,800
Fuel Weight (*lbs*)	290,900	273,600
Fuel Wt / Gross Wt	50.2%	50.1%
Wing Area (ft^2)	9,108	9,693
Wing Weight (*lbs*)	81,900	68,070
Aspect Ratio	2.36	1.59
Range (*n.mi.*)	5,260.0	5,494.6
Landing angle of attack	11.35°	11.99°
$(L/D)_{max}$	9.473	9.588

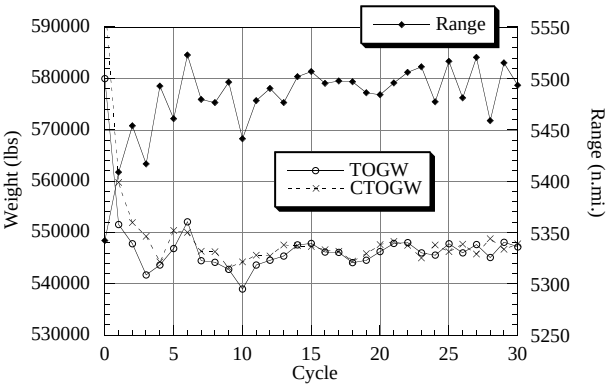

Figure 7: Convergence of Case 27a

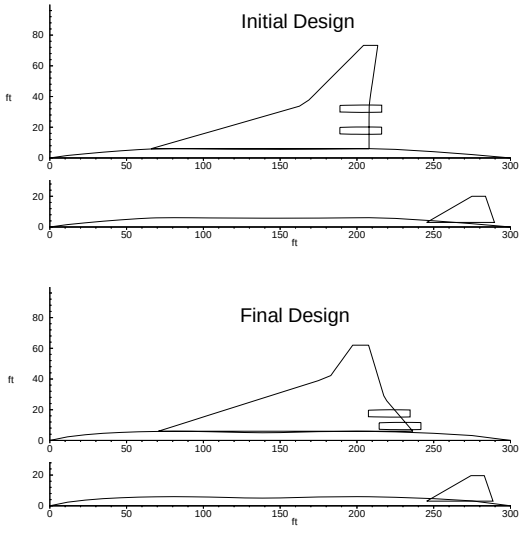

Figure 8: Initial and final planforms, Case 27a

50 *ft/sec.* These changes increased the range by over 80 *n.mi.* In addition to the three constraint violations mentioned previously, the engine out limit is violated. The engines are too far out for the vertical tail to trim in an emergency. After 30 optimization cycles, the TOGW has been reduced by 32,700 *lbs* with all of the constraints satisfied. A convergence history of the TOGW is shown in Fig. 7. The initial and final planforms are shown in Fig. 8 and Table 6 compares the two designs.

The vertical tail initially increased in size to satisfy the engine out constraint, but was reduced as the engines continued to move inboard, see Fig. 9. In this case, more weight is saved by moving the engines in and reducing the vertical tail size than by taking advantage of wing bending moment relief to reduce the wing weight. In the final design, the engines are moved in as far as the constraints allow. This results in a slightly heavier wing compared to Case 26a. But this also allows a small vertical tail to be used to satisfy the engine out constraint. The weight penalty for going to this design is very small, about 0.27% of the TOGW.

The stability and control derivatives were estimated using the interlacing technique. This technique worked well, and examples are shown in Fig. 10 for one stability derivative and in Fig.11 for one control derivative. The jumps that occur every five cycles are the updated derivatives from Kay's code. The estimations for C_{l_β} show the greatest differences, although the magnitude of the jumps is not larger than the jumps in the other derivatives.

6.2.2. Case 27b

It seemed odd that the optimizer moved the engines inboard, reducing the wing bending moment relief and resulting in a heavier wing. So we performed a second optimization, Case 27b, using the

Table 6: Comparison of Initial and Final Designs, Case 27a

	Initial	Final
Gross Weight (*lbs*)	580,000	547,300
Fuel Weight (*lbs*)	290,900	272,800
Fuel Wt / Gross Wt	50.2%	49.8%
Wing Area (ft^2)	9,108	9,808
Wing Weight (*lbs*)	81,900	70,060
Aspect Ratio	2.36	1.57
Vertical Tail Area (ft^2)	450.0	431.0
Vertical Tail Weight (*lbs*)	1,730	1,640
Nacelle 1 position, y (*ft*)	17.8	9.4
Nacelle 2 position, y (*ft*)	32.1	17.6
Range (*n.mi.*)	5,342.4	5,493.4
Landing angle of attack	11.35°	11.99°
$(L/D)_{max}$	9.239	9.577

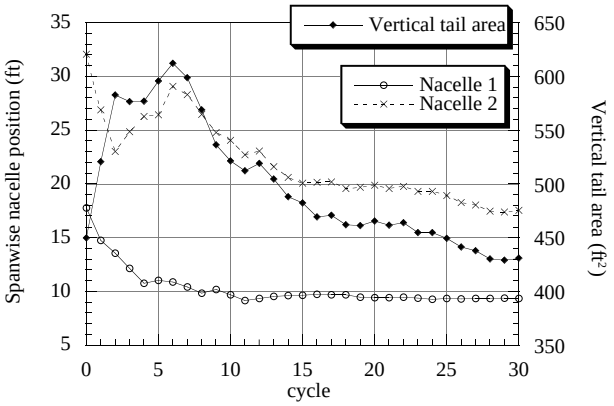

Figure 9: History of nacelle positions and vertical tail area, Case 27a

same initial design as Case 27a, but we started with a larger vertical tail. There was initially no violation of the engine out constraint. This allowed the engines to remain well outboard where there is a larger wing bending moment relief effect.

The optimal design occurred after only 11 optimization cycles, but due to noisy derivatives, the optimizer slowly wandered away from this design. The optimal design has a TOGW of 543,700 *lbs*, a reduction of 37,700 *lbs* from the initial design. Thus, the changed initial condition allowed the optimizer to find a minimum 0.66% TOGW less than Case 27a, and 0.38% TOGW less than our optimized baseline, Case 26a. These changes are probably within the *noise* of the methodology. The initial and final planforms are shown in Fig. 12 and Table 7 compares the two designs.

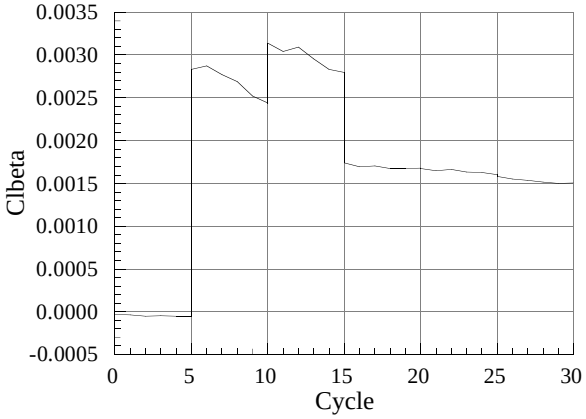

Figure 10: History of C_{l_β} for Case 27a

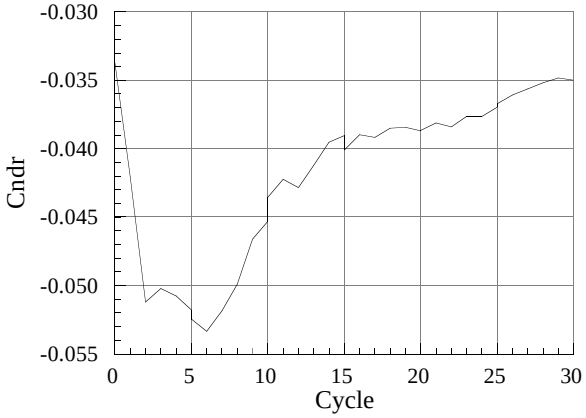

Figure 11: History of $C_{n_{\delta r}}$ for Case 27a

The range decreased by 100 *n.mi.* when the vertical tail size was increased by 400 ft^2. This is due to the increased drag from the larger tail. Although this seems like a large penalty, the final design is slightly better than the Case 27a final design. The nacelles are split because the vertical tail must balance the net yawing moment. Thus, the net yawing moment will remain the same by moving nacelle 1 in and nacelle 2 out by equal distances. These cases show our derivative based optimization is very susceptible to local minima. Also, these two cases indicate that nacelle position is not a design driver and nacelles can be placed using other considerations, such as landing gear interference with inlet flow or rotor burst.

The most critical constraints for the final design are range and the engine out constraint. Some of the section C_ℓ constraints and the landing angle of attack constraint are also critical. Also important in this design is fuel volume, nacelle strike on the inboard nacelle, and minimum wing t/c.

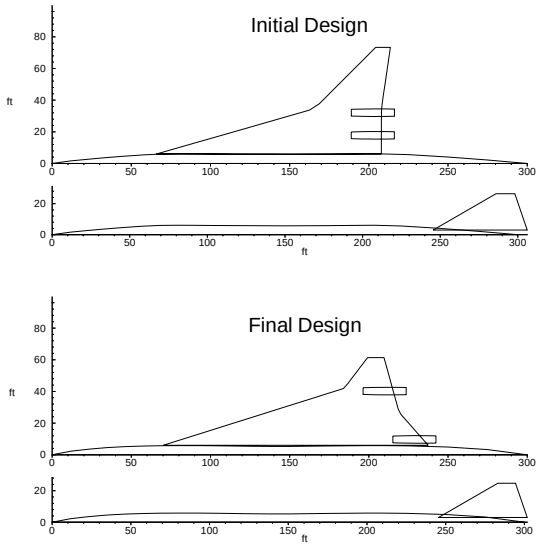

Figure 12: Initial and final planforms, Case 27b

Table 7: Comparison of Initial and Final Designs, Case 27b

	Initial	Final
Gross Weight (*lbs*)	581,400	543,700
Fuel Weight (*lbs*)	290,900	272,100
Fuel Wt / Gross Wt	50.0%	50.0%
Wing Area (ft^2)	9,108	9,870
Wing Weight (*lbs*)	82,010	67,940
Aspect Ratio	2.36	1.53
Vertical Tail Area (ft^2)	850.0	734.8
Vertical Tail Weight (*lbs*)	2,970	2,570
Nacelle 1 position, y (*ft*)	17.8	9.7
Nacelle 2 position, y (*ft*)	32.1	40.2
Range (*n.mi.*)	5,242.7	5,499.0
Landing angle of attack	11.39°	11.99°
$(L/D)_{max}$	9.092	9.574

6.3. Vertical and Horizontal Tail Considerations

Next we added horizontal tail sizing to our optimization. This increased the number of design variables to 28 and the number of constraints to 67. The constraints added are the takeoff rotation constraint, the approach trim constraint and a constraint to prevent the wing and horizontal tail from overlapping.

6.3.1. Case 28a

The starting design from Case 27a is used, with the addition of a horizontal tail. Adding the horizontal tail only increased the weight by 9,000 *lbs*, but the additional drag caused a 400 *n.mi.* reduction in the range. This design satisfies the three additional constraints for the horizontal tail.

The weight of the final design is 630,000 *lbs*, an increase of over 40,000 *lbs* from the starting weight, and more than 80,000 *lbs* heavier than the previous optimized designs. Most of this weight increase is fuel weight. Almost 70,000 *lbs* more fuel is required for this design than for Case 27a. The planforms are all very similar, although the trailing edge is somewhat less swept in this case.

The initial and final planforms are shown in Figure 13 and Table 8 compares the two designs[†] The convergence histories for TOGW and range are shown in Fig. 14 and the horizontal tail size history is shown in Fig. 15. The noisy convergence is a product of our variable complexity modeling and the noisy analysis.

For the final design, range and landing angle of attack are again the critical constraints. There are a number of constraints which were important, but not critical, to this design. These include fuel volume, section C_ℓ, time required to rotate, minimum nacelle spacing, the engine out limit, and maximum thrust required during the cruise-climb.

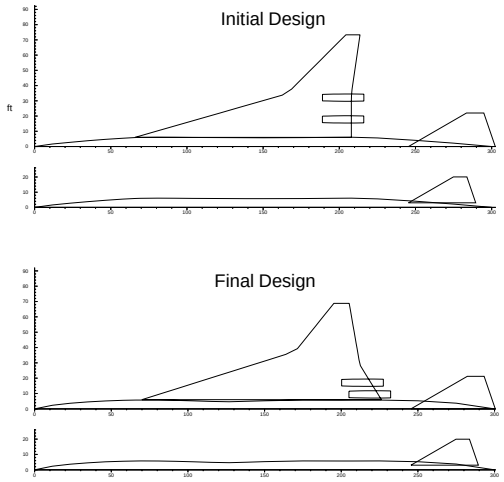

Figure 13: Initial and final planforms, Case 28a

6.3.2. Case 28b

We performed another optimization using the same initial design variables, but increasing the size and thrust of the engines, and reducing $(T/W)|_{eng}$ by one, to see the effects of engine technology. Engine thrust increased from 39,000 *lbs* to 46,000 *lbs* per

[†]Crisafulli *et al.*[25] found that reducing the trailing edge flap deflection to 20° from the value of 30° had the effect of reducing the trailing edge sweep to near zero.

Table 8: Comparison of Initial and Final Designs, Case 28a

	Initial	Final
Gross Weight (*lbs*)	589,200	630,000
Fuel Weight (*lbs*)	290,900	340,200
Fuel Wt / Gross Wt	50.0%	54.0%
Wing Area (ft^2)	9,108	9,713
Wing Weight (*lbs*)	82,630	77,720
Aspect Ratio	2.36	1.95
Vertical Tail Area (ft^2)	450.0	447.1
Vertical Tail Weight (*lbs*)	1,740	1,760
Nacelle 1 position, y (*ft*)	17.8	9.4
Nacelle 2 position, y (*ft*)	32.1	17.1
Horz. Tail Area (ft^2)	1,500.0	1,400.1
Horz. Tail Weight (*lbs*)	7,930	7,510
Time to rotate (*sec*)	4.56	4.67
Range (*n.mi.*)	4,935.9	5,465.2
Landing angle of attack	11.27°	11.97°
$(L/D)_{max}$	8.709	8.711

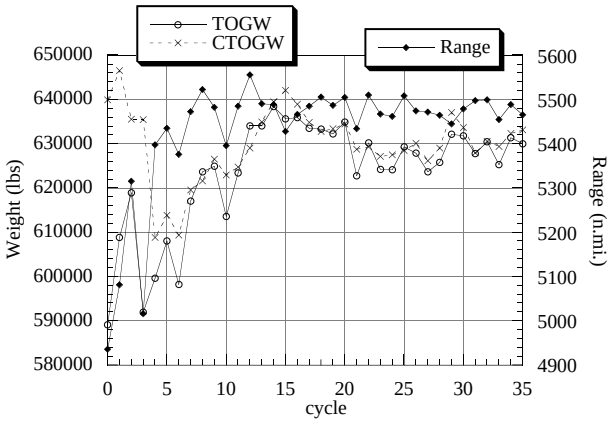

Figure 14: Takeoff Gross Weight and Range convergence, Case 28a

engine, nacelle diameter and length increased from 5 *ft* and 27 *ft* to 6.5 *ft* and 35 *ft*, respectively. This increased the propulsion system weight by over 28,000 *lbs* and the TOGW by about 35,600 *lbs*. Also, the range decreased by 436 *n.mi.*, although the drag on the aircraft only increased by about two counts. The initial weight of this design is only about 5,000 *lbs* less than the optimized design in the previous case, but the range is 1,000 *n.mi.*less than our required range.

After 40 optimization cycles, our TOGW is 755,400 *lbs*. Although this could be a poor local minimum, this large increase in weight can be explained. With no other changes, the large range deficiency would require approximately 100,000 *lbs* of fuel to

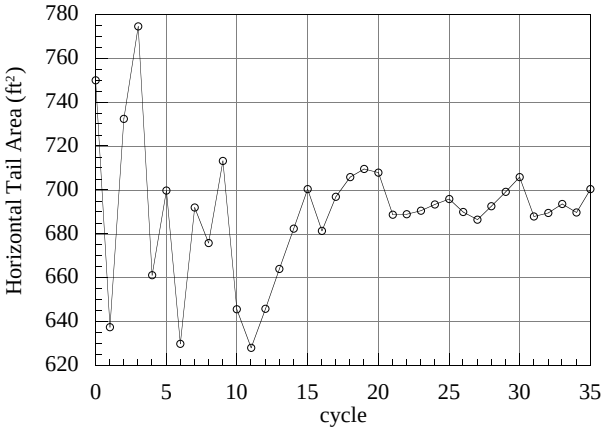

Figure 15: Horizontal Tail Size convergence, Case 28a

satisfy the range constraint. Adding this much fuel weight would cause numerous other constraint violations, such as the thrust constraints, the fuel volume constraint, the landing angle of attack, and the takeoff rotation constraint. Satisfying these constraints would further increase the weight. The actual increase in fuel weight is about 118,000 *lbs*.

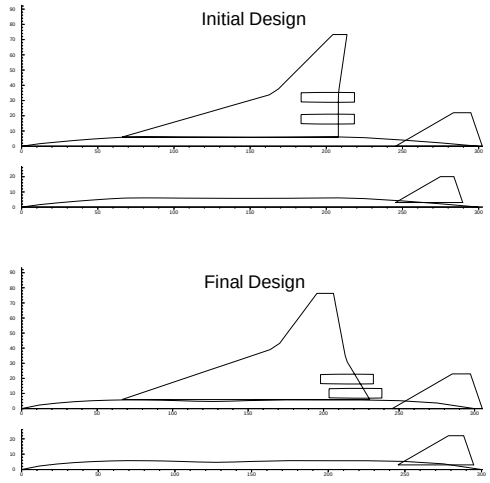

Figure 16: Initial and final planforms, Case 28b

The final planform is very similar to our previous designs, but the wing is much bigger. The initial and final planforms are shown in Fig. 16. These designs are also compared in Table 9. In this design, range, landing angle of attack, section C_ℓ, and the engine out limit are the critical constraints. Once again, fuel volume, inboard nacelle strike, time to rotate, and maximum thrust required for cruise-climb are the other important constraints.

Table 9: Comparison of Initial and Final Designs, Case 28b

	Initial	Final
Gross Weight (*lbs*)	624,800	755,400
Fuel Weight (*lbs*)	290,900	408,600
Fuel Wt / Gross Wt	50.0%	54.0%
Wing Area (ft^2)	9,108	11,193
Wing Weight (*lbs*)	84,300	95,800
Aspect Ratio	2.36	2.08
Vertical Tail Area (ft^2)	450.0	564.6
Vertical Tail Weight (*lbs*)	1,770	2,270
Nacelle 1 position, y (*ft*)	17.8	10.1
Nacelle 2 position, y (*ft*)	32.1	19.5
Horz. Tail Area (ft^2)	1,500.0	1,647.1
Horz. Tail Weight (*lbs*)	8,030	9,150
Time to rotate (*sec*)	4.47	4.68
Range (*n.mi.*)	4,500.6	5,471.9
Landing angle of attack	12.26°	12.00°
$(L/D)_{max}$	8.573	8.684

6.4. Engine Sizing (Case 29a)

Our next optimization included engine sizing, as well as the vertical and horizontal tail sizing. This added one design variable, up to 29, and one constraint, up to 68. The balanced field length constraint of 10,000 *ft* is the additional constraint. Cases 28a and 28b both violate this constraint considerably with balanced field lengths of 11,650.9 *ft* and 12794.3 *ft*, respectively. The initial design for this case is the final design from case 28b.

The final design is much heavier than the initial design. The weight increases by 110,000 *lbs*. The final design has a much larger wing. Wing area increases by 1,569 *ft* and wing weight increases by over 33,000 *lbs*. Increasing the wing area often reduces the wing loading, which decreases the balanced field length, but in this case, the wing loading increases from 59.04 lbs/ft^2 to 60.22 lbs/ft^2. This is a relatively small increase in wing loading and it allows a smaller, lighter wing to be used.

To satisfy the balanced field length constraint the thrust to weight ratio is increased by 13.5%, from 0.244 to 0.277. This is accomplished by increasing the thrust per engine by almost 14,000 *lbs*. Increasing the thrust causes the propulsion system weight to increase by almost 25,000 *lbs*. Clearly, the balanced field length constraint was a critical requirement. As shown below, relaxing the BFL constraint to 11,000 *ft* results in a large weight savings, and the 10,000 *ft* requirement may be too restrictive.

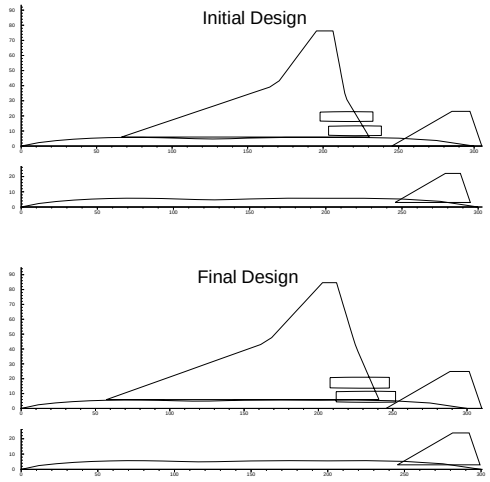

Figure 17: Initial and final planforms, Case 29a

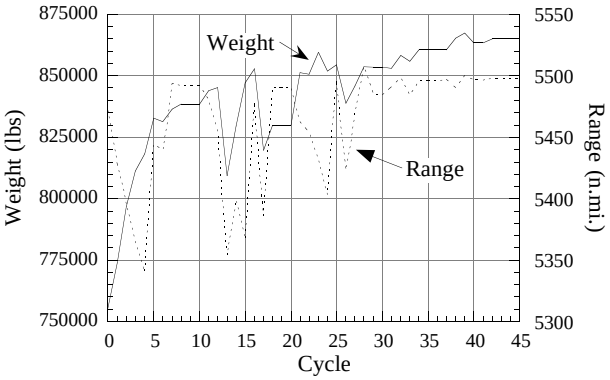

Figure 18: Takeoff Gross Weight and Range convergence, Case 29a

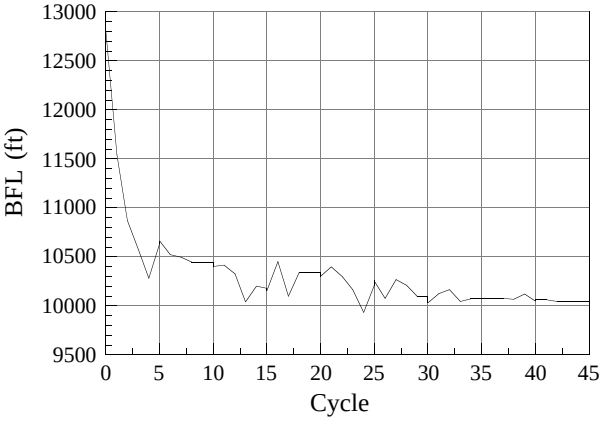

Figure 19: Balanced field length convergence, case 29a

For the final design, the constraints on range, nacelle strike, BFL, and the engine out condition were

Table 10: Comparison of Initial and Final Designs, Case 29a

	Initial	Final
Gross Weight (*lbs*)	755,400	865,000
Fuel Weight (*lbs*)	408,600	453,800
Fuel Wt / Gross Wt	54.1%	52.5%
Wing Area (ft^2)	12,794	14,363
Wing Weight (*lbs*)	95,780	129,200
Aspect Ratio	2.08	2.00
Vertical Tail Area (ft^2)	564.6	670.5
Vertical Tail Weight (*lbs*)	2,270	2,740
Nacelle 1 position, y (*ft*)	10.1	7.9
Nacelle 2 position, y (*ft*)	19.5	17.3
Horz. Tail Area (ft^2)	1,646.6	1,924.3
Horz. Tail Weight (*lbs*)	9,150	10,990
Time to rotate (*sec*)	4.68	4.95
Engine thrust (*lbs*)	46,000	59,798
Nacelle length (*ft*)	35.00	39.91
Nacelle diameter (*ft*)	6.50	7.41
Propulsion system weight (*lbs*)	77,290	101,200
Range (*n.mi.*)	5,472.1	5,500.1
Landing angle of attack	12.00°	10.62°
Balanced Field Length (*ft*)	12,794	10,044
$(L/D)_{max}$	8.684	9.000

all critical. The nacelle strike constraint is limiting the landing angle of attack in this case. The BFL constraint sizes the engine, and the engine out condition sizes the vertical tail. The constraints on maximum thrust required, section C_ℓ, time to rotate, and horizontal tail/wing overlap were nearly critical. The horizontal tail is sized by the time to rotate constraint.

The initial and final planforms are shown in Fig. 17 and the designs are compared in Table 10. The convergence is very noisy between cycles 10 and 30, but improves dramatically for cycles 30 to 45, as can be seen in Fig. 18. Figure 19 shows the history of the balanced field length.

6.5. Subsonic Leg (Case 29b)

For this optimization, we added a subsonic leg to our mission requirement. We required the initial 500 *n.mi.* be flown at Mach 0.9 and then continue on with the supersonic cruise-climb. This did not add any design variables, but did require two more constraints. The additional constraints require that the available thrust be greater than the required thrust for the subsonic leg and the transition from the subsonic to supersonic leg. In this optimization, the transition is an instantaneous jump. The addition of these constraints results in 29 design variables and 70 constraints.

The initial design for this case is the final design from Case 29a. After adding the subsonic leg to the mission, the range for this design dropped to 5,221.5 *n.mi.*, a 280 *n.mi.* decrease. The range constraint is the only constraint which is initially violated.

The optimizer had trouble improving the range without violating the BFL constraint. Many attempts were made using different move limits to find a design which would satisfy both constraints. The final design satisfies both constraints, but weighs 100,000 *lbs* more than the initial design.

Seventy percent of the increase in weight is due to added fuel. Another 20% of the increase comes from increased wing weight. The rest of the weight increase comes from various sources, including the vertical tail, horizontal tail, and the propulsion system.

The final design does not appear too different from the initial design. There is an increase in aspect ratio which improves the subsonic aerodynamic performance. Figure 20 shows both the starting and ending designs and Table 11 compares them. The convergence histories of TOGW, range, and BFL are shown in Figures 21 and 22.

The increase in weight agrees with trends predicted in other studies. A study by the Douglas Aircraft Company[48] showed large increases in weight with increasing subsonic mission segments. Martin *et al.*[49] also predicted increases in weight corresponding to increasing subsonic leg.

The actual subsonic leg requirements for an HSCT could be less than the 500 *n.mi.* that we have used. Reducing this requirement would make it easier for the optimizer to find a feasible design. An increase in the allowable BFL could also help the optimizer.

6.6. Sensitivity To Parameters and Analysis Accuracy

6.6.1. Engine Sizing with Relaxed BFL Constraint (Case 29c)

This optimization study was conducted to investigate the effect of relaxing the BFL constraint on the engine size and overall aircraft parameters, including the TOGW and horizontal and vertical tail sizes. Since this requirement was one of the most critical, resulting in a very large increase in TOGW, we decided to investigate the design sensitivity to the BFL.

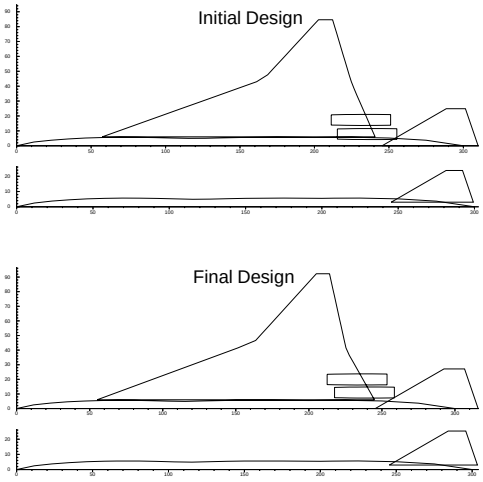

Figure 20: Initial and final planforms, Case 29b

Table 11: Comparison of Initial and Final Designs, Case 29b

	Initial	Final
Gross Weight (*lbs*)	865,000	966,400
Fuel Weight (*lbs*)	453,800	523,900
Fuel Wt / Gross Wt	52.5%	54.2%
Wing Area (ft^2)	14,363	15,610
Wing Weight (*lbs*)	129,200	148,900
Aspect Ratio	1.99	2.18
Vertical Tail Area (ft^2)	670.5	778.2
Vertical Tail Weight (*lbs*)	2,740	3,210
Nacelle 1 position, y (*ft*)	7.9	11.0
Nacelle 2 position, y (*ft*)	17.3	19.9
Horz. Tail Area (ft^2)	1,924.3	2,293.4
Horz. Tail Weight (*lbs*)	10,990	13,400
Time to rotate (*sec*)	4.95	4.86
Engine thrust (*lbs*)	59,798	62,972
Nacelle length (*ft*)	39.91	40.95
Nacelle diameter (*ft*)	7.41	7.61
Propulsion system weight (*lbs*)	101,200	107,200
Range (*n.mi.*)	5,221.5	5,519.2
Landing angle of attack	10.62°	10.25°
Balanced Field Length (*ft*)	10,047	9,984
$(L/D)_{max}$	8.998	8.953

The number of design variables (29) and the values and number of constraints (68) were unchanged compared to Case 29a, and the only difference was that the value of the BFL constraint was changed to 11,000 *ft* from the value of 10,000 *ft* used in Case 29a. The initial design for this case was one of the intermediate designs from the optimization run 29a.

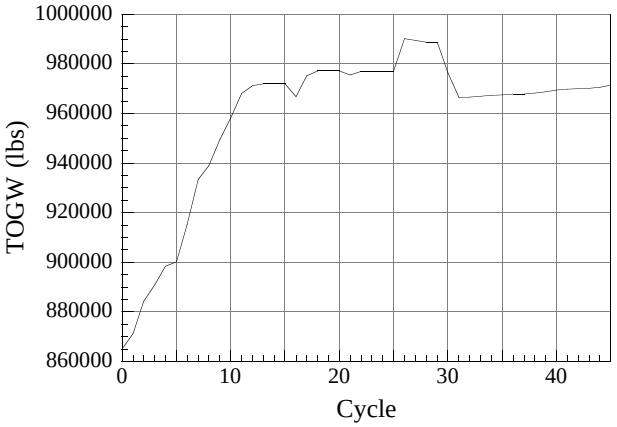

Figure 21: Takeoff Gross Weight convergence, Case 29b

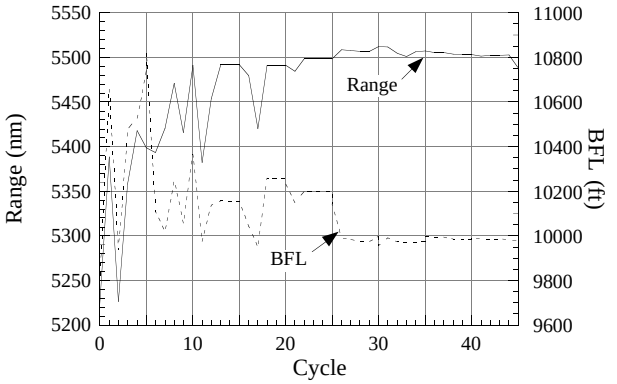

Figure 22: Range and BFL convergence, Case 29b

The resulting 11,000 *ft* BFL design, Case 29c, is compared to the 10,000 *ft* BFL design, Case 29a, in Table 12. The planforms are compared in Fig. 23. For Case 29c the constraints of range, nacelle strike, wing and horizontal tail overlap, bank angle and the engine out condition were all critical. Interestingly, the BFL constraint is not critical any more, and engine sizing is done by the requirements on the thrust at cruise. The rotation time constraint determines the horizontal tail size, and vertical tail size is determined by the engine out condition.

The significant weight and size reductions of the HSCT from Case 29a to 29c are readily apparent in Table 12. TOGW is reduced by over 92,000 *lbs* and fuel weight is reduced by over 50,000 *lbs*. The wing area decreases by 1,172 ft^2, vertical tail area decreases by 216.4 ft^2 and horizontal tail area decreases by 429.9 ft^2. Relaxing the BFL constraint made it non-critical for the thrust requirements, which led to engine sizing based on the cruise thrust requirement, thus decreasing the size and weight of the engines.

Table 12: Comparison of Final Designs for Case 29a and 29c

	Case 29a	Case 29c
Gross Weight (*lbs*)	865,000	772,981
Fuel Weight (*lbs*)	453,800	403,346
Fuel Wt / Gross Wt	52.5%	52.1%
Wing Area (ft^2)	14,363	13,191
Wing Weight (*lbs*)	129,200	113,086
Aspect Ratio	2.00	1.99
Vertical Tail Area (ft^2)	670.5	454.1
Vertical Tail Weight (*lbs*)	2,740	1,898
Nacelle 1 position, y (*ft*)	7.9	7.08
Nacelle 2 position, y (*ft*)	17.3	14.41
Horz. Tail Area (ft^2)	1,924.3	1,494.4
Horz. Tail Weight (*lbs*)	10,990	8,346
Time to rotate (*sec*)	4.95	5.27
Engine thrust (*lbs*)	59,798	49,258
Nacelle length (*ft*)	39.91	37.40
Nacelle diameter (*ft*)	7.41	6.95
Propuls. system weight (*lbs*)	101,200	82,791
Range (*n.mi.*)	5,500.1	5,502.9
Landing angle of attack	10.62°	10.58°
Balanced Field Length (*ft*)	10,044	10,922
$(L/D)_{max}$	9.000	9.155

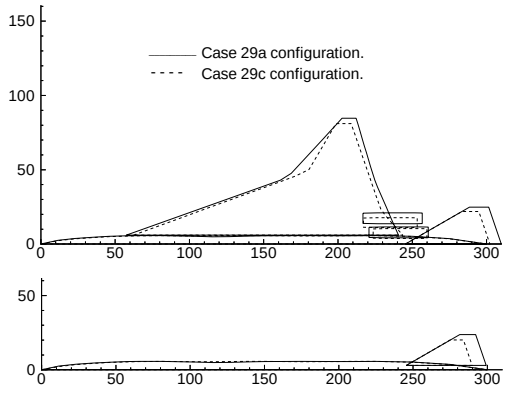

Figure 23: Comparison of planforms for Case 29a and 29c.

Propulsion weight was reduced by 18,409 *lbs* and engine thrust reduced by 10,540 *lbs*. Reduced engine thrust also led to reduced vertical tail size, which is driven by the engine out condition. The overall reduction of weight and inertia moments resulted in considerably reduced horizontal tail area, which is driven by the rotation time constraint.

6.6.2. TOGW Sensitivity to Drag Change

A series of optimization runs was made to investigate the sensitivity of take-off weight of the HSCT to changes in drag estimation. Several reasons led to this investigation, among which were the uncertainty of the drag coefficient values when using simplified aerodynamics equations, and the need to assess the penalty in TOGW with changes in trim drag. Work by Knill *et al.*[18] suggested that the current drag estimation methods differed from more accurate calculations by around 2 counts.

For this investigation it was decided to use the Case 29c configuration as the baseline and then perform optimization studies while changing friction drag values slightly. Four different optimized designs were obtained during the investigation, with drag changes of -2, -1, +1 and +2 counts. The starting point for all four designs was the final configuration of Case 29c. Changes were made in the friction drag subroutine so that the drag coefficient over the entire flight profile was changed. Convergence was reached in about 25 optimization cycles for the reduced drag designs and in about 35 cycles for the increased drag designs.

In all four cases the optimizer converged to different configurations, which can be seen in Figures 24 to 27. The new planforms are plotted along with the baseline configuration for comparison. Configurations for -1 and +1 drag count change are very close to the baseline planform. However, as expected, the weight decreases with a decrease in drag and increases with an increase in drag. Table 13 tabulates the results. The configurations for -2 and +2 drag counts show a clear tendency to change the wing sweep with a change in drag. Increased drag causes the optimizer to reduce the drag by using a wing planform with more sweep to get better supersonic performance to compensate for the drag penalties. When the drag was decreased the optimizer took advantage of the improved performance and chose a wing planform with less sweep to reduce wing weight.

The results of this study illustrate the difficulty of performing optimization studies with typical real-life analysis methods and with a significant number of design variables and constraints. Because of the fine-grain noise from the analysis methods and the likely non-convex design space associated with the design variables and constraints, smooth variations of the results with the change in drag were not obtained. Nevertheless, trends can be identified. Figure 28 shows the TOGW found by the MDO design procedure for the different drag increments. Although

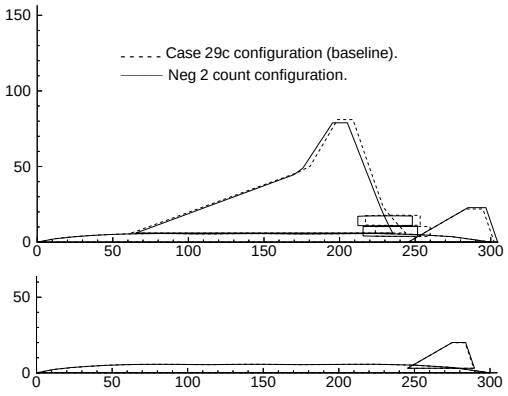

Figure 24: Baseline and negative 2 drag count planforms

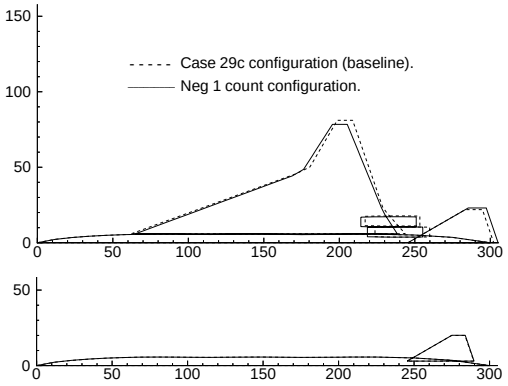

Figure 25: Baseline and negative 1 drag count planforms

not smooth, the plot shows large weight penalties for the optimized designs with small changes in drag. The extreme sensitivity may be in part explained by the degraded engine technology used in the baseline Case 29c, which results in a design very near the limits of an achievable design.

Figures 29 to 30 show how some of the design parameters change with the drag change. Note that the lines do not represent continuous functions of drag and are drawn only to help in visualizing the trends.

Examining the plots one can see that most of the TOGW increase is due to the extra fuel weight necessary to compensate for the range deficiency because of the extra drag. Structural weight of the HSCT changes very little, as can be seen on the wing weight plot, Fig. 29, even though the size of the aircraft is slightly larger for greater drag (wing area 13,387 ft^2

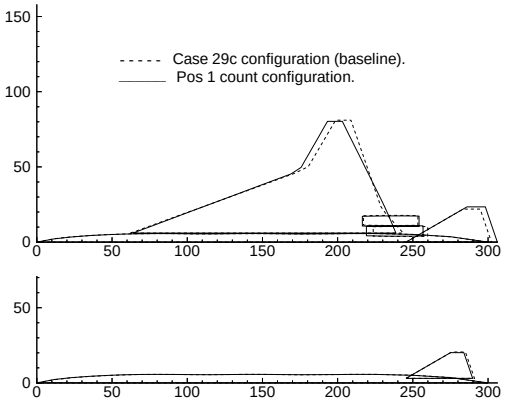

Figure 26: Baseline and positive 1 drag count planforms

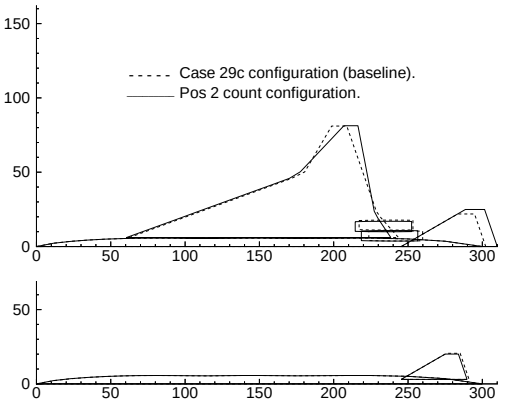

Figure 27: Baseline and positive 2 drag count planforms

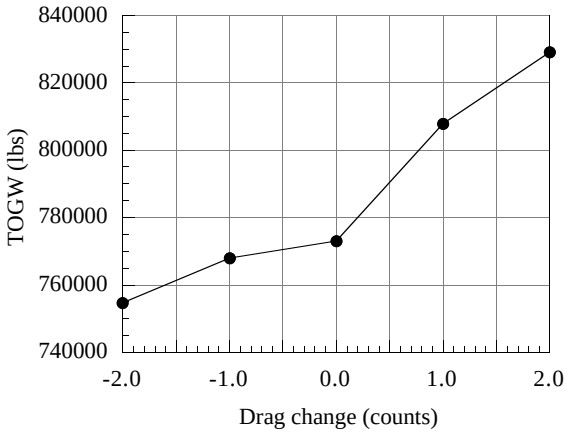

Figure 28: TOGW variation for changed drag designs

Table 13: Comparison of the baseline design (Case 29c) to the changed drag designs

	-2 counts	-1 count	baseline	+1 count	+2 counts
Gross Weight (*lbs*)	754,560	767,907	772,981	807,774	829,099
Fuel Weight (*lbs*)	391,817	401,316	403,346	426,628	440,564
Fuel Wt / Gross Wt	51.93%	52.3%	52.1%	52.82%	53.14%
Wing Area (ft^2)	12,476	12,597	13,191	13,153	13,387
Wing Weight (*lbs*)	107,071	107,364	113,086	115,077	119,053
Aspect Ratio	2.00	1.95	1.99	1.96	1.975
Root wing thickness (%)	2.52	2.50	2.48	2.46	2.63
L.E. break wing thickness(%)	1.85	1.80	1.77	1.84	1.75
Tip wing thickness (%)	1.70	1.69	1.59	1.65	1.59
Vertical Tail Area (ft^2)	444.5	449.2	454.1	479.3	481.9
Vertical Tail Weight (*lbs*)	1,851	1,877	1,898	2,014	2,039
Nacelle 1 position, y (*ft*)	7.17	7.10	7.08	7.43	7.21
Nacelle 2 position, y (*ft*)	14.1	13.8	14.41	13.91	13.46
Horz. Tail Area (ft^2)	1,616.8	1,650.8	1,494.4	1,706.8	1,932.8
Horz. Tail Weight (*lbs*)	8,986	9,208	8,346	9,617	10,946
Engine thrust (*lbs*)	48,835	50,554	49,258	53,309	54,155
Prop. system weight (*lbs*)	81,992	84,989	82,791	89,873	91,416
Range (*n.mi.*)	5,503.9	5,499.4	5,502.9	5,498.2	5,493.1
Landing angle of attack	10.93°	11.17°	10.58°	11.14°	11.09°
Balanced Field Length (*ft*)	10,947	10,988	10,922	10,979	10,963
$(L/D)_{max}$	9.165	9.055	9.155	8.940	8.892

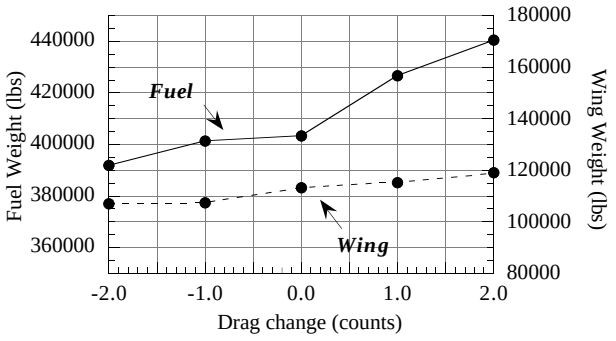

Figure 29: Fuel and wing weight variation for changed drag designs

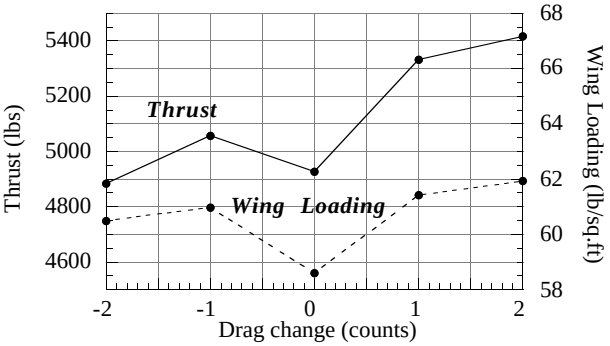

Figure 30: Engine thrust and wing loading variation for changed drag designs

for +2 drag count configuration versus 12,476 ft^2 for -2 drag count). Engine thrust, however, does increase with drag, as can be expected, to compensate for poorer take-off performance and increased cruise drag, as shown in Fig. 30). Out of the 74,539 *lbs* weight increase from -2 to +2 count designs, the contribution of the fuel weight is 48,747 *lbs* (65.4%), the contribution of the propulsion system weight is 9,424 *lbs* (12.6%), and the wing weight contributes 11,982 *lbs* (16.1%), with the other 4,386 *lbs* (5.9%) coming from the other components (tails, fuselage, etc.).

Figure 28 suggests that the baseline design, with no change in drag, is inconsistent with all the other results and possibly represents a different local minimum. Several attempts to recompute the results for the changed drag cases with different starting points failed to change them appreciably.

6.6.3. TOGW Sensitivity to Rotation Time (Case 29d)

The rotation time in all previous cases was restricted to 5 seconds. The choice of this value, although reasonable, is somewhat arbitrary. Occasionally, the five second constraint could not be met. Therefore, it was decided to investigate the effect of changing the rotation time constraint on the TOGW and other parameters of the HSCT. Two optimization runs were conducted for this purpose, with the rotation time set to 6 seconds (Case 29d-6) and with the rotation time set to 20 seconds (Case 29d-20). All the rest of the constraints and requirements were the same as for Case 29c (relaxed BFL case).

The two optimizations were started from the same initial point as the baseline design (Case 29c). The final configurations are compared with the baseline in Figures 31 and 32. Some major parameters of the designs are compared in Table 14.

As one can see, the TOGWs of both new designs (*6 sec* and *20 sec*) are slightly larger than that of the baseline configuration (779,358 and 774,134 *lbs*), even though we expected the TOGW to decrease. This indicated that the rotation time constraint was not critical for finding the optimum HSCT for these conditions. Observe that in Table 14 the actual rotation time of the new designs is 5.81 sec for the *6 sec* design, and 5.63 sec for the *20 sec* design. Clearly, the rotation time constraint was not active in either case and, in these cases, had no effect on the final configurations of HSCT. The fact that the new designs have heavier weights may again be explained by the complex design space, which, along with the noise in the system, allows the optimizer to settle in a local minimum.

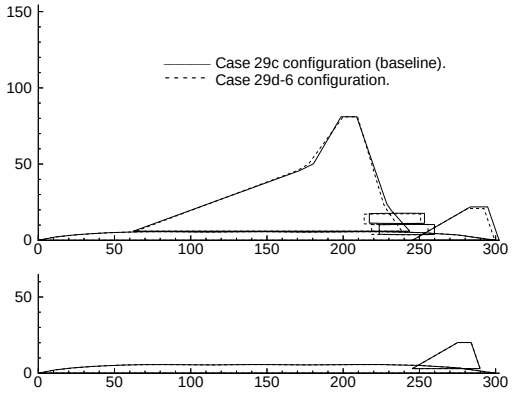

Figure 31: Configurations for Cases 29c and 29d-6

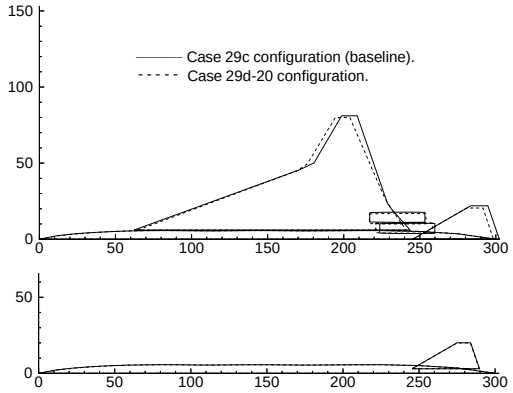

Figure 32: Configurations for Cases 29c and 29d-20

7. Summary and Conclusions

Multidisciplinary design optimization using variable complexity modeling can produce feasible, optimized designs satisfying important constraints associated with real aircraft design. We have extended our code to include these constraints and explored design issues which are often not considered at this level of aircraft design. A summary of the optimization cases studied, together with the resulting TOGWs, is shown in Table 15.

These essential trim and control constraints make a large difference to the resulting HSCT design. Adding the engine-out constraint forces the vertical tail to be sized based on the engine location. We found that the spanwise engine location is constrained by the aerodynamic control requirements. Generally

Table 14: Comparison of Final Designs for Case 29d and 29c, used to study the effect of the rotation time constraint.

	Case 29d-6	Case 29d-20	Case 29c
Gross Weight (*lbs*)	779,358	774,134	772,981
Fuel Weight (*lbs*)	407,523	403,910	403,346
Fuel Wt / Gross Wt	52.3%	52.18%	52.1%
Wing Area (ft^2)	12,956	12,916	13,191
Wing Weight (*lbs*)	112,254	110,290	113,086
Aspect Ratio	2.03	1.98	1.99
Vertical Tail Area (ft^2)	456.8	450.7	454.1
Vertical Tail Weight (*lbs*)	1,913	1,887	1,898
Nacelle 1 position, y (*ft*)	7.09	7.39	7.08
Nacelle 2 position, y (*ft*)	14.0	13.4	14.41
Horz. Tail Area (ft^2)	1,350.8	1,301.2	1,494.4
Horz. Tail Weight (*lbs*)	7,557	7,269	8,346
Time to rotate (*sec*)	5.81	5.63	5.27
Engine thrust (*lbs*)	51,391	51,856	49,258
Propulsion system weight (*lbs*)	86,463	87,233	82,791
Range (*n.mi.*)	5,503.5	5,495.2	5,502.9
Landing angle of attack	10.80°	10.92°	10.58°
Balanced Field Length (*ft*)	11,035	10,913	10,922
$(L/D)_{max}$	9.079	9.064	9.155

Table 15: Summary of optimizations

Case	Additional Requirement	TOGW (*lbs*)
26a	None (baseline case)	545,800
27a	Vertical tail sizing	547,300
27b	Vertical tail sizing	543,700
28a	Horizontal tail sizing	630,000
28b	Reduced engine technology	755,400
29a	Balanced field length	865,000
29b	Subsonic leg	966,400
29c	Relaxed BFL	772,981
	Changed drag:	
	-2 counts	754,560
	-1 count	767,907
	+1 count	807,774
	+2 counts	829,099
29d	Changed rotation time:	
	6 seconds	779,358
	20 seconds	774,134

the engines are placed as far inboard as the nacelle lateral spacing constraints allow, and the vertical tail size is minimized. But, as was shown in Case 27b, there is another local minimum which has a larger vertical tail and one nacelle located on the outboard wing section. This takes advantage of the greater bending moment relief effect, which lowers the wing weight by about 2,000 *lbs*.

The inboard nacelle strike constraints were active in every case. In the first five cases, it is not clear what these constraints affected. It is possible that these constraints limit the amount of trailing edge sweep in those cases. In the last two cases, 29a and 29b, these constraints limit the allowable landing angle of attack.

The horizontal tail size is based on the requirement that the aircraft must rotate to the take-off position in under 5 *sec*, except for Cases 29d. The tail size required to do this is highly dependent on the landing gear location (tipback angle). The tail deflection for approach trim was not critical for any of our designs.

The increased vertical tail size and the addition of a horizontal tail increases the TOGW directly by only 2.5%, but they result in drag penalties, which translate to large increases in weight. This increased weight is mostly fuel. Although we found that trim and control increased the weight, adding these con-

siderations provides a more realistic model and better designs.

Reducing the technology level of the engines $[\Delta(T/W)|_{eng} = -1]$ caused a large increase in engine weight and size. This caused a large decrease in range and a large weight penalty was incurred to satisfy the constraints with reduced engine technology. Engine sizing was added along with the BFL requirement. The requirement of a 10,000 *ft* BFL was found to be very restrictive, and caused a very large increase in TOGW.

Adding a 500 *n.mi.* subsonic leg to our mission caused a large decrease in total range. Overcoming this range deficit while maintaining the 10,000 *ft* BFL requirement was difficult. The final design was much heavier than the starting design. Although this design is extremely heavy, it demonstrates that our MDO technique is capable of producing successful designs, even when faced with very difficult requirements.

Sensitivity studies showed the dependence of the TOGW and other parameters on the balanced field length and the rotation time constraints, and also the effect of small changes in the drag estimates. Relaxing the BFL constraint from 10,000 *ft* to 11,000 *ft* reduced the TOGW by over 90,000 *lbs*. The parametric drag study showed a large weight decrease with decrease in drag coefficient. The difference in TOGW between the -2 count and +2 count designs was 74,539 *lbs*, with most of the weight increase being contributed by the fuel weight change (48,747 *lbs* or 65.4%). Finally, the relaxed rotation time constraint did not impact the HSCT configuration and TOGW.

Acknowledgement

The work reported here was supported by NASA Langley Research Center under grant NAG1-1160 and is gratefully acknowledged.

References

[1] Sobieszczanski-Sobieski, J., "Multidisciplinary Optimization of Engineering Systems: Achievements and Potential," in *Proceedings of an International Seminar, Optimization: Methods and Applications, Possibilities and Limitations* (Bergmann, H. W., ed.), vol. 47 of *Lecture Notes in Engineering*, pp. 42–62, Berlin, Germany: Springer-Verlag, 1989.

[2] Sobieszczanski-Sobieski, J., "Multidisciplinary Design Optimization: An Emerging New Engineering Discipline," in *presented at The World Congress on Optimal Design of Structural Systems*, (Rio de Janeiro, Brazil), Aug. 1993.

[3] Sobieszczanski-Sobieski, J. and Haftka, R. T., "Multidisciplinary Aerospace Design Optimization: Survey of Recent Developments," AIAA Paper 96-0711, Jan. 1996.

[4] Giunta, A., Golovidov, O., Knill, D., Grossman, B., Mason, W., Watson, L., and Haftka, R., "Multidisciplinary Design Optimization of Advanced Aircraft Configurations," Keynote paper at the 15th *International Conference on Numerical Methods in Fluid Dynamics*, Monterey, CA, (to appear in *Lecture Notes in Physics*, Springer-Verlag), June 26 1996. Also MAD Center Report 96-06-01, Virginia Tech, AOE Dept., Blacksburg, VA, June 1996.

[5] Hutchison, M. G., Unger, E., Mason, W. H., Grossman, B., and Haftka, R. T., "Variable-Complexity Aerodynamic Optimization of a High Speed Civil Transport Wing," *Journal of Aircraft*, vol. 31, pp. 110–116, January-Febuary 1994.

[6] Hutchison, M. G., Huang, X., Mason, W. H., Haftka, R. T., and Grossman, B., "Variable-Complexity Aerodynamic-Structural Design of a High-Speed Civil Transport Wing," AIAA Paper 92-4695, Sept. 1992.

[7] Hutchison, M. G., Mason, W. H., Grossman, B., and Haftka, R. T., "Aerodynamic Optimization of an HSCT Configuration Using Variable-Complexity Modeling," AIAA Paper 93-0101, Jan. 1993.

[8] Dudley, J., Huang, X., Haftka, R. T., Grossman, B., and Mason, W. H., "Variable-Complexity Interlacing of Weight Equation and Structural Optimization for the Design of the High-Speed Civil Transport," AIAA Paper 94-4377, Sept. 1994.

[9] MacMillin, P. E., Dudley, J., Mason, W. H., Grossman, B., and Haftka, R. T., "Trim, Control and Landing Gear Effects in Variable-Complexity HSCT Design," AIAA Paper 94-4381, Sept. 1994.

[10] Wakayama, S. and Kroo, I., "Subsonic Wing Planform Design Using Multidisciplinary Optimization," *Journal of Aircraft*, vol. 32, pp. 746–753, July-August 1990.

[11] Gallman, J. W., Smith, S. C., and Kroo, I. M., "Optimization of Joined-Wing Aircraft," *Journal of Aircraft*, vol. 30, pp. 897–905, November-December 1993.

[12] Braun, R., Kroo, I., and Sobieski, I., "Implementation and Performance Issues in Collaborative Optimization," AIAA Paper 96-4017, pp. 295–305, Sept. 1996.

[13] Marris, D., Bandte, O., and Schrage, D., "Application of Probabilistic Methods for the Determination of an Economically Robust HSCT Configuration," AIAA Paper 96-4090-CD, pp. 968–978, Sept. 1996.

[14] Röhl, P., Morris, D., and Schrage, D., "HSCT Wing Design Through Multilevel Decomposition," AIAA Paper 95-3944, Sept. 1995.

[15] Sellar, R., Batill, S., and Renaud, J., "Response Surface Based Concurrent Subspace Optimization for Multidisciplinary System Design," 34th AIAA Aerospace Sciences Meeting and Exhibit, AIAA Paper 96-0714, Reno, NV, Jan. 1996.

[16] Tzong, G., Baker, M., Yalamanchili, K., and Giesing, J., "Aeroelastic Loads and Structural Optimization of a High Speed Civil Transport Model," AIAA Paper 94-4378, Sept. 1994.

[17] Borland, C. J., Benton, J. R., Frank, P. D., Kao, T. J., Mastro, R. A., and Barthelemy, J.-F. M., "Multidisciplinary Design Optimization of a Commercial Aircraft Wing—an Exploratory Study," AIAA Paper 94-4305, Sept. 1994.

[18] Knill, D. L., Balabanov, V., Golovidov, O., Grossman, B., Mason, W. H., Haftka, R. T., and Watson, L. T., "Accuracy of Aerodynamic Predictions and its Effects on Supersonic Transport Design," MAD Center Report 96-12-01, Virginia Tech, AOE Dept., Blacksburg, VA, Dec. 1996.

[19] MacMillin, P., Golovidov, O., Mason, W., Grossman, B., and Haftka, R., "Trim, Comtrol and Performance Effects in Variable-Complexity High-Speed Civil Transport Design," MAD Center Report 96-07-01, July 1996, http://www.aoe.vt.edu/mad/Publications/reports/96/rep1.html.

[20] McCullers, L. A., "Aircraft Configuration Optimization Including Optimized Flight Profiles," in *Proceedings of Symposium on Recent Experiences in Multidisciplinary Analysis and Optimization* (Sobieski, J., ed.), NASA CP-2327, pp. 396–412, Apr. 1984.

[21] Kay, J., Mason, W. H., Durham, W., and Lutze, F., "Control Authority Assessment in Aircraft Conceptual Design," AIAA Paper 93-3968, Aug. 1993.

[22] Kay, J., Mason, W., Durham, W., Lutze, F., and Benoliel, A., "Control Power Issues in Conceptual Design: Critical Conditions, Estimation Methodology, Spreadsheet Assessment, Trim and Bibliography," VPI-Aero-200, Nov. 1993, http://www.aoe.vt.edu/aoe/faculty/Mason_f/SD1.html.

[23] Giunta, A., Balabanov, V., Haim, D., Grossman, B., Mason, W., Watson, L., and Haftka, R., "Wing Design for a High-Speed Civil Transport Using a Design of Experiments Methodology," AIAA Paper 96-4001, Proceedings of the 6th AIAA/NASA/ISSMO Symposium on Multidisciplinary Analysis and Optimization, pp. 168–183, Sept. 1996. http://www.aoe.vt.edu/mad/Publications/96/papers96.html.

[24] Kaufman, M., Balabanov, V., Burgee, S., Giunta, A., Grossman, B., Haftka, R., Mason, W., and Watson, L., "Variable-complexity response surface approximations for wing structural weight in HSCT design," *Computational Mechanics*, vol. 18, pp. 112–126, June 1996.

[25] Crisafulli, P., Kaufman, M., Giunta, A., Mason, W., Grossman, B., Watson, L., and Haftka, R., "Response Surface Approximations for Pitching Moment, Including Pitch-Up, in the MDO Design of an HSCT," AIAA Paper 96-4136, Proceedings of the 6th AIAA/NASA/ISSMO Symposium on Multidisciplinary Analysis and Optimization, pp. 1308–1322, Sept. 1996. http://www.aoe.vt.edu/aoe/faculty/Mason_f/MRRpubs96.html.

[26] Sliwa, S. M., "Impact of Longitudinal Flying Qualities Upon the Design of a Transport With Active Controls," AIAA Paper 80-1570, 1980.

[27] Sliwa, S. M., "Sensitivity of Optimal Preliminary Design of a Transport to Operational Constraints and Performance Index," AIAA Paper 80-1895, Aug. 1980.

[28] McCarty, C. A., Feather, J. B., Dykman, J. R., Page, M. A., and Hodgkinson, J., "Design and Analysis Issues of Integrated Control Systems for High-Speed Civil Transports," NASA Contractor Report 186022, May 1992.

[29] Anderson, M. A. and Mason, W., "An MDO Approach to Control-Configured-Vehicle Design," AIAA Paper 96-4058, Proceedings of the 6th AIAA/NASA/ISSMO Symposium on Multidisciplinary Analysis and Optimization, Bellevue, WA, pp. 734–743, Sept. 1996. http://www.aoe.vt.edu/aoe/faculty/Mason_f/MRRpubs96.html.

[30] Anderson, M., Suchkov, A., Einthoven, P., and Waszak, M., "Flight Control System Design Risk Assessment," AIAA Paper 95-3197, AIAA Guidance, Navigation and Control Conference, Aug. 1995.

[31] Chai, S. and Mason, W., "Landing Gear Integration in Aircraft Conceptual Design," AIAA Paper 96-4038, Proceedings of the 6th AIAA/NASA/ISSMO Symposium on Multidisciplinary Analysis and Optimization, pp. 525–540, Sept. 1996. http://www.aoe.vt.edu/aoe/faculty/Mason_f/SD1.html.

[32] Torenbeek, E., *Synthesis of Subsonic Airplane Design*. Delft University Press, 1982.

[33] FAA, Washington, DC, *FAR Part 25*.

[34] Ogburn, M. E., Foster, J. v., Pahle, J. W., Wilson, R. J., and Lackey, J. B., "Status of the Validation of High-Angle-of-Attack Nose-Down Pitch Control Margin Design guidelines," AIAA Paper 93-3623, 1993.

[35] Benoliel, A., "Aerodynamic Pitch-Up of Cranked Arrow Wings: Estimation, Trim, and Configuration Design," Master's thesis, Virginia Tech, 1994.

[36] Benoliel, A. and W.H.Mason, "Pitch-Up Characteristics for HSCT Class Planforms: Survey and Estimation," AIAA Paper 94-1819,AIAA 12th Applied Aerodynamics Conference, Colorado Springs, CO, June 1994.

[37] Craidon, C. B., "Description of a Digital Computer Program for Airplane Configuration Plots," NASA TM X-2074, 1970.

[38] Barnwell, R., "Approximate Method for Calculating Transonic Flow About Lifting Wing-Body Configurations," NASA TR R-452, pp. 58–61, Apr. 1976.

[39] Hutchison, M., Unger, E., Mason, W. H., Grossman, B., and Haftka, R., "Variable-Complexity Aerodynamic Optimization of an HSCT Wing Using Structural Wing-Weight Equations," AIAA Paper 92-0212, Jan. 1992.

[40] Eminton, E., "On the Minimisation and Numerical Evaluation of Wave Drag," Royal Aircraft Establishment Report AERO.2564, Nov. 1955.

[41] Grandhi, R. V., Thareja, R., and Haftka, R. T., "NEWSUMT-A: A General Purpose Program for Constrained Optimization using Constraint Approximations," *ASME Journal of Mechanisms, Transmissions, and Automation in Design*, no. 107, pp. 94–99, 1985.

[42] Bertin, J. and Smith, M., *Aerodynamics for Engineers*. Prentice Hall, 2 ed., 1989.

[43] Carlson, H., Mack, R., and Barger, R., "Estimation of Attainable Leading Edge Thrust for Wings at Subsonic and Supersonic Speeds," NASA TP-1500, 1979.

[44] Carlson, H. and Miller, D., "Numerical Methods for the Design and Analysis of Wings at Supersonic Speeds," NASA TN D-7713, 1974.

[45] Harris, Jr., R. V., "An Analysis and Correlation of Aircraft Wave Drag," NASA TM X-947, 1964.

[46] Hoak, D. E. *et al.*, *USAF Stability and Control DATCOM*. Flight Control Division, Air Force Flight Dynamics Laboratory, WPAFB, Ohio, 45433-0000, 1978. Revised.

[47] Roskam, J., *Methods for Estimating Stability and Control Derivatives of Conventional Subsonic Airplanes*. Kansas: Roskam Aviation and Engineering Corporation, 1971.

[48] Douglas Aircraft Company, "Study of High-Speed Civil Transports," NASA Contractor Report 4235, p. 105, 1989.

[49] Martin, G. L., Beissner Jr., F. L., Domack, C. S., and Shields, E. W., "The Influence of Subsonic Mission Segments on the Use of Variable-Sweep Wings for High Speed Civil Transport Configurations," AIAA Paper 88-4470, Sept. 1988.